Energy 79 (2015) 149–162

Contents lists available at ScienceDirect

Energy

journal homepage: www.elsevier.com/locate/energy

Optimization of carbon-capture-enabled coal-gas-solar power generation

Philip G. Brodrick [a], Charles A. Kang [a], Adam R. Brandt [a, *], Louis J. Durlofsky [a]

[a] Department of Energy Resources Engineering, Stanford University, Stanford, CA 94305-2220, USA

ARTICLE INFO

Article history:
Received 2 July 2014
Received in revised form
29 October 2014
Accepted 1 November 2014
Available online 9 December 2014

Keywords:
Optimization
Carbon capture
Solar thermal
Natural gas combined cycle

ABSTRACT

Computational optimization is used to determine the optimal design and time-varying operations of a carbon dioxide capture retrofit to a coal-fired power plant. The retrofit consists of an amine-based temperature-swing absorption system, to which process steam is supplied from an auxiliary unit. Two candidate auxiliary heat sources are explored: natural gas and solar thermal. The NPV (net present value) of the retrofitted facility is maximized to determine which auxiliary system is preferable, under a variety of economic conditions. Optimized NPV is found to be most sensitive to the price of natural gas and the electricity price. At an 8% real discount rate, without renewable energy incentives, natural gas prices must be high (in excess of 10 USD/GJ) for a solar thermal design to be preferable, and electricity prices must reach ≈55 USD/MWh in order for solar-thermal-based designs to have a positive NPV. Incentives such as investment tax credits and solar power purchase agreements can make solar-thermal-based designs preferable to natural-gas-based designs under certain circumstances.

1. Introduction

CCS (carbon capture and storage) is expected to be a "critical component" in the portfolio of measures applied to address climate change [1]. To date, technical challenges and a lack of regulatory certainty have hindered CCS deployment. Recent studies, however, suggest that several CCS technologies may be commercialized in the next 10–20 years [2]. This work focuses on ABTSA (amine-based temperature-swing absorption) systems, which are the most mature CCS technology due to their history of use in natural gas sweetening [3].

ABTSA systems require large capital investment and a substantial amount of low-temperature steam for the desorption of CO_2 (approximately 3.6 MJ/tonne CO_2 [4]). This steam can be extracted from the power plant itself, or can be provided by an adjacent auxiliary system. Auxiliary systems have several advantages. First, reductions in the base-plant electricity output are avoided (these reductions range from 24 to 40% of plant capacity) [3,5]. In fact, depending on the design, auxiliary systems can increase overall electricity generation from the facility. Additionally, fewer alterations to the base-plant are required, which may make the retrofit process simpler. Finally, any fuel source can be used to generate the required steam, allowing for the integration of renewable energy sources.

This work explores the optimal design and time-varying operations of an auxiliary CCS facility. Two heat sources are explored – natural gas and solar thermal. The use of solar thermal systems mitigates concerns about increased energy consumption associated with CCS [6]. While net energy consumption clearly increases, fossil energy consumption remains unchanged. However, if the (optimal) economics of solar thermal auxiliary systems are less favorable than those of corresponding natural gas systems, they are less likely to be utilized. In order to identify the optimal system configuration under a range of possible economic scenarios, computational optimization is utilized to determine high-level system design and operations of the major retrofit components.

Optimizing facility operations has been shown to decrease the cost of CCS-enabled power generation. Chalmers et al. [7] demonstrated the technical feasibility of flexible operation in carbon capture systems, and Cohen et al. [8] found substantial benefits from optimizing the operations of a parasitic ABTSA system. By including both the design and operations in the optimization procedure, further economic benefits have been demonstrated. Mac Dowell and Shah [9] optimized the design and operation of a parasitic ABTSA system in order to minimize the total annualized cost, and found benefits from operating the capture system

* Corresponding author. Tel.: +650 724 8251; fax: +650 725 2099.
E-mail address: abrandt@stanford.edu (A.R. Brandt).

http://dx.doi.org/10.1016/j.energy.2014.11.003
0360-5442/

intermittently at higher capture rates. Khalilpour [10] utilized coupled design and operations optimization to maximize NPV (net present value) of solvent-based post combustion capture. Khalilpour additionally developed a multilevel decision-making methodology.

CCS facilities using auxiliary natural gas systems have also been studied. Bashadi and Herzog [11] explored three different natural gas system configurations and determined that in some situations, auxiliary systems could be preferable to parasitic systems. Optimization of these auxiliary natural-gas-based CO_2 capture systems has also been performed. Kang et al. [12] optimized the time-dependent system operations of an ABTSA system with a natural-gas-based auxiliary heat supply, and found an increase in operating profit of up to 20% compared to heuristic operations. This work was extended [13] to additionally include the optimization of facility design. Through application of bi-objective optimization, Kang et al. [13] determined the optimal trade-off between the capital investment requirement for a CCS retrofit and the NPV from the facility, given different natural gas and electricity price scenarios.

Solar thermal auxiliary CCS systems have also been studied. Cohen et al. [14] explored high-temperature, high-efficiency solar thermal auxiliary systems at various carbon tax rates, and concluded that without a high carbon tax, the direct use of a solar thermal system for power generation was more profitable. Li et al. [15] explored multiple locations and solar thermal design costs, and concluded that the cost of a non-concentrating vacuum tube would have to fall below 90 USD/m^2, and a concentrating parabolic trough system would have to fall below 150 USD/m^2, for the cost of electricity to be lower than it would be in a parasitic system. Mokhtar et al. [16] utilized an iterative search to explore solar thermal system designs with fixed operations, and concluded that solar collectors would have to decrease to 100 USD/m^2 under 2009 conditions for the system to have a positive NPV. To date, computational optimization has not been used to determine optimal design and operations of auxiliary solar thermal CCS systems.

While both solar thermal and natural gas auxiliary CCS systems have been considered independently, the two have not been compared within a consistent modeling framework, as is accomplished in this study. In addition, previous work [13] on the optimal design and operations of natural gas auxiliary systems utilized price–duration curves to account for variable operations, which did not enable certain time-dependent effects, such as the storage of CO_2-rich amine, to be incorporated into the modeling. Such effects are included in this work. Also, while the existing literature on solar thermal auxiliary systems has examined a variety of configurations and costs [14,15], the low efficiency/low cost systems considered here have yet to be explored. Our optimizations are performed with various fuel prices, electricity prices, discount rates, and solar incentives, with the goal of determining the optimal facility for a variety of plausible economic conditions.

This paper proceeds as follows. In Section 2, the overall problem setup is presented, and descriptions of the models and optimization parameters for each of the major facility subsystems are provided. The optimization methodology is discussed in Section 3. In Section 4, we present our procedure for clustering time-varying data to create a small number of representative days, which is necessary to render the optimization problem computationally tractable. Results for a wide range of scenarios are presented in Section 5. We conclude with a summary and suggestions for future work in Section 6. Additional details on the optimization of the heat recovery steam generator are provided in the online Supplementary Information.

2. System model

Our system is modeled as a set of interacting subsystems. Fig. 1 illustrates the mass flows between systems, and indicates the decision variables that determine the characteristics of each module. Two categories of decision variables enter the formulation: design variables ($\mathbf{x}$), which specify component sizes and configurations, and hourly operational variables ($\mathbf{u}$), which govern mass flow rates throughout the system over a set of representative days. The combination of these two types of decision variables allows for the calculation of the NPV of the entire facility, which is maximized by the optimization algorithm (described in Section 3). We first provide an overview of the general problem setup, and we then describe the natural gas, solar thermal, and CO_2 capture subsystems. Variables are defined when first used, and key variables are listed in the Nomenclature section.

In this work, we represent the auxiliary natural gas plant, auxiliary solar thermal system, and CPP (coal-fired power plant) as a series of modules that interact by exchanging energy and mass flows. The mathematical model entails a set of coupled algebraic equations describing mass and energy balances for each component. For the capture model, the quantities required are extracted from the IECM 8.0.2 modeling software [17,18], as described in Section 2.4. The models for the CPP, auxiliary natural gas plant (including heat recovery steam generator), and CO_2 capture subsystems are essentially identical to those used in Kang et al. [12,13]. Those references (including the online Supplementary Material [13]) should be consulted for full details. The solar thermal system assessed here has not, to our knowledge, been previously considered for use in a CCS retrofit.

2.1. General problem setup

We consider a 440 MW CPP that provides base-load power and is being retrofit for CCS. For simplicity, we assume that the CPP has a 100% capacity factor. The capital cost of the CPP is assumed to have been recovered, but capital investment in carbon capture systems and auxiliary heat units is included in the NPV calculation. The CPP, assumed to be located in Farmington, New Mexico, exports power to Southern California. Presently, two GW-scale power plants (the 2.04 GW Four Corners Power Plant, and the 1.9 GW San Juan Generating Station) exist at this location and have exported a sizeable fraction of their electricity to Southern California in recent history. Largely due to California law SB 1368[1], a greenhouse gas emissions regulation which limits the annual average emissions intensity to 499 kg CO_2/MWh, much of this power is no longer exported to California. In our model, we consider CPP retrofits using ABTSA, with the goal of reducing the emission intensity to meet this standard.

Two different options are considered for supplying auxiliary heat for CCS: using natural gas as fuel, and using a solar thermal array. As indicated in Fig. 1, the steam from either or both subsystems can be sent to the reboiler in the capture subsystem regeneration column, and upon return the condensate is split such that mass is conserved in each subsystem. If both auxiliary systems are active, the steam streams can be combined after each is expanded to the required (reboiler) pressure and temperature. Both auxiliary systems can produce electricity, but we assume that the electricity production is not large enough to influence the electricity price. Consistent with this assumption, we limit the total

[1] This type of regulation is not unique to California. Oregon, New York, and Washington all have similar standards in effect. Additionally, new federal regulations will place a similar limit on new CPPs.

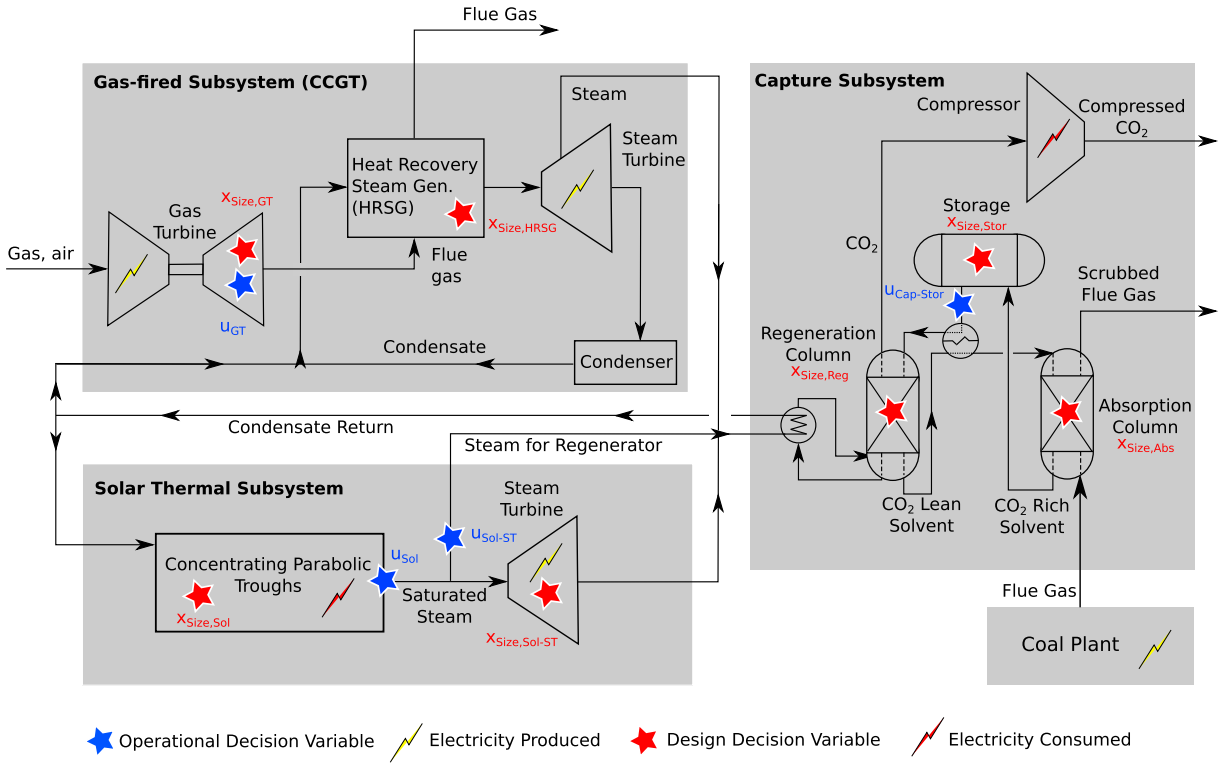

Fig. 1. System diagram showing design decision variables (**x**) and operational decision variables (**u**), which are described in Section 2. Mass flows shown are intended to indicate the destination of each stream, not to indicate physical pipe systems.

electricity production of the overall plant to be at most 7700 GWh/y, which is twice the production of the existing CPP. This limit also prevents a facility design where the primary purpose of the retrofit is capacity expansion, which otherwise might occur under certain economic conditions. The focus of the problem is instead on steam production for solvent regeneration in the capture system, while still allowing the auxiliary system to co-produce electricity.

The capital costing methods used in the natural gas and carbon capture subsystems are based on the methods applied by Kang et al. [13], which are in turn based on the Guthrie method [19–21]. Using this approach, PECs (purchased equipment costs) are calculated based on the exponential scaling of a reference unit [19,21], as given by:

$$\frac{\mathrm{PEC}}{\mathrm{PEC}_{\mathrm{ref}}} = \left(\frac{S}{S_{\mathrm{ref}}}\right)^{\alpha} \tag{1}$$

where S is the component size, the subscript ref indicates a reference component, and α is the system scaling factor. These PECs are adjusted for escalation and then multiplied by a component specific module factor to account for installation costs, a 1.18 contingency and fee coefficient, and a 1.3 auxiliary facility factor. Interest during construction is then applied to the resulting total capital cost [13,19–21]. The solar thermal subsystem cost is based on reported data and does not use the Guthrie method. All capital expenditures are depreciated for tax purposes according to the MACRS (Modified Accelerated Cost Recovery System) [22].

2.2. Gas-fired subsystem

The natural gas subsystem model is based on that used by Kang et al. [13]. It is comprised of four main components: a gas turbine, an HRSG (heat recovery steam generator), a steam turbine, and a condenser. The gas turbine is modeled using (algebraic) mass and energy balances. The energy conversion rate for the gas turbine is given by:

$$\dot{E} = \eta_{\mathrm{th}}\, \eta_{\mathrm{rel}}(L)\, \dot{m}_g(L)\, \Delta h_g \tag{2}$$

where $\dot{E}$ (W) is the work output from the gas turbine, η_{th} is the design thermal efficiency, η_{rel} is the efficiency loss due to partial loading, L is the partial load, $\dot{m}_g$ (kg/s) is the flue gas flow rate, and Δh_g (MJ/kg) is the natural gas HHV (higher heating value). The efficiency loss due to partial load is a function of L as determined by Kim [23]. The fuel used by the gas turbine is assumed to be a mixture of 72.9% CH_4, 25.9% C_2H_6, and 1.2% N_2 (by mass), with an HHV of 53,900 kJ/kg. Gas turbine specifications are summarized in Table 1.

Designing an HRSG to optimally produce process heat for carbon capture, itself a complex problem, has been explored in detail [13]. Optimizing the entire set of HRSG design decision variables described in Kang et al., while also optimizing time-dependent operations, would however be very computationally expensive. In this work, the design of the natural gas subsystem is instead determined through a "pre-optimization" procedure. In this approach, described in the Supplementary Information, the full set

Table 1
Gas turbine thermodynamic data.

Property	Value
HHV efficiency	36.7%
Gas turbine outlet temperature[a]	921 K
Specific power[b]	489 kJ/kg
Fuel HHV	53.9 MJ/kg

[a] Assuming inlet air temperature of 298 K.
[b] Per kg of working fluid.

of optimal HRSG design decision variables is determined at several different discount rates. The HRSG configuration resulting from these optimizations is then used in subsequent optimization runs. The particular configuration specified depends only on the discount rate. This approach enables us to describe the gas-fired subsystem design using only three decision variables, which we now discuss.

The first variable, $x_{Num,GT}$, is an integer variable that specifies the number of gas-fired subsystems built. The second and third variables, which are both continuous, define the overall gas turbine capacity ($x_{Size,GT}$) and the size of the HRSG components relative to this overall capacity ($x_{Size,HRSG}$). The size of the steam turbine is determined from the maximum amount of steam that the HRSG can generate, and the condenser size is calculated from the cooling demand for the steam turbine, as in Kang et al. [13]. System operations are controlled through a set of time-dependent decision variables for the partial-loading of the gas turbine ($\mathbf{u}_{GT}$).

Capital costs for the gas-fired subsystem are based on data provided by Ulrich and Vasudevan [19]. Systems designed with these costs were shown to match published values for actual constructed facilities [24] in Kang et al. [13]. The cost of the gas turbine and condenser are calculated using Equation (1), with values shown in Table 2. We use linear cost scaling for the HRSG, as in Casarosa et al. [25], with purchased equipment PEC_{ref} values given in Table 3.

2.3. Solar thermal subsystem

The solar thermal subsystem used in this work is based on the GlassPoint system [26–28], which was designed to provide process steam for enhanced oil recovery projects. The system generates saturated steam at 138 bar (336 °C) from feed water provided at up to 80 °C. Compared to conventional solar thermal systems, the GlassPoint design sacrifices peak efficiency to reduce manufacturing costs. The system uses light-weight parabolic mirrors which are placed inside a slightly pressurized greenhouse to protect them from dust and wind. System maintenance is, consequently, readily automated, which reduces operation and maintenance costs. A 7 MW installation in Oman is shown in Fig. 2.

The ideal solar thermal system for the direct production of process steam for carbon capture would provide saturated steam at the conditions required by the capture system (≈3 bar, 135 °C) [17,18]. While the GlassPoint system provides heat with lower exergy than is typical for large-scale solar thermal operations, the pressure is substantially higher than that required for solvent regeneration in the CO_2 capture system. In order to take advantage of this excess energy, we incorporate a wet steam turbine into the solar thermal subsystem. This turbine expands the steam from 138 bar to 3 bar as needed for solvent regeneration.

Table 2
Gas turbine and steam cycle PEC data.

Equipment	S_{ref}	PEC_{ref} (USD)	α
Gas turbine	200 MW	47,300,000	0.77
Steam turbine	17.5 MW	115,000	0.89
Electrical generator	1 MW	65,000	0.95
Condenser	900 m^2	70,000	0.75

Table 3
HRSG PEC data.

Equipment	PEC_{ref} (USD/m^2)	α
Economizer	45.7	1
Evaporator	34.9	1
Superheater	96.2	1
Reheater	56.2	1

Wet steam turbines are commonly used in industrial applications where saturated steam, which cannot be utilized effectively in a traditional steam turbine due to damage from high rates of condensation, is available at higher pressures than required. While they operate at lower efficiencies than traditional steam turbines (an isentropic efficiency of 65% is used for the wet steam turbine, as opposed to the ≈85% of typical condensing steam turbines), wet steam turbines provide an option for reducing system exergy destruction.

The steam produced by the solar thermal system is determined based on data provided by GlassPoint [28]. The amount of heat generated by a facility is assumed to scale linearly with global minus diffuse irradiation at the location of the facility [28]. Annual heat generation from two existing installations in California is paired with the average irradiation at each site: heat generation of 101 Wh/m^2 and irradiation of 363 Wh/m^2 near Daggett, and heat generation of 85.3 Wh/m^2 and irradiation of 273 Wh/m^2 near Bakersfield. In Farmington, New Mexico, the site used in this model, the average irradiation is 346 Wh/m^2, for which we interpolate an annual heat generation of 98 Wh/m^2. This annual heat generation is used in conjunction with the facility size in a particular design to determine the amount of annual steam produced (given the enthalpy difference between the GlassPoint inlet and outlet conditions). Steam production on an hourly basis is determined by multiplying the annual steam production by the ratio of the irradiation in a given hour to the net annual irradiation (where irradiation in both cases is global minus diffuse).

We assume in this work that the GlassPoint system could be modified to produce 100% saturated steam, rather than the 80% cited in their reports [17,18], while still maintaining the same overall efficiency. Unlike typical GlassPoint installations that utilize produced formation water with high levels of contaminants, our focus here is on closed-looped systems with low levels of impurities. The reduction in impurities leads to decreased scaling with higher quality steam, which makes this assumption reasonable.

The solar thermal subsystem is described with two design decision variables and two sets of operational decision variables. The design decision variables are both continuous, and indicate the size of the parabolic trough system ($x_{Size,Sol}$) and the size of the wet steam turbine ($x_{Size,Sol-ST}$). Both of these variables are bounded inclusively by zero, with a value of zero meaning the system is not built. The first set of operational decision variables ($\mathbf{u}_{Sol}$) determines the fraction of steam that is utilized from the solar thermal system in each time interval. The second set of decision variables ($\mathbf{u}_{Sol-ST}$) defines the fraction of the utilized steam that is passed through the wet steam turbine, with the remainder sent directly to the capture system.

Information regarding the capital cost of the solar thermal subsystem was provided by GlassPoint [28]. The main cost of the system is the fixed cost, which includes costs for the construction of the parabolic troughs and greenhouses, and for the wet steam turbine and associated electrical generator. Complete operations costs[2] (dominated by pumping) are included, but are small in comparison, roughly 40 cents/GJ at 2010 electricity prices. Table 4 shows the dominant costs and scaling factors.

2.4. CO_2 capture subsystem

The capture subsystem modeled in this work is composed of four main components: absorption, regeneration, amine storage, and compression. The system uses MEA (monoethanolomine) as

[2] This includes operations and maintenance costs, as well as price-dependent electrical costs for pumping.

Fig. 2. A 7 MW GlassPoint solar thermal installation in Oman [26].

Table 4
Solar thermal cost data.

Equipment	S_{ref}	PEC_{ref}[a]	α
Parabolic troughs	1 m^2	200 USD/m^2	1
Wet steam turbine[b]	17.5 MW	115,000 USD	0.89
Electrical generator	1 MW	65,000 USD	0.95

[a] Total cost for parabolic troughs, PECs for wet steam turbine and electrical generator.
[b] Data from conventional steam turbines.

the solvent, with a weight concentration of 30%. MEA is used exclusively in cost calculations of the storage system. Other system components are parameterized from the default amine CO_2 capture system for a pulverized coal plant in IECM 8.0.2 [17,18]. Energy requirements for the capture subsystem are dominated by the regeneration heat requirement, as shown in Table 5.

The capture system design is characterized by the capacities of the absorption, regeneration, and solvent storage systems, which are all treated as continuous decision variables. The decision variables for the absorption and regeneration systems ($x_{Size,Abs}$ and $x_{Size,Reg}$ respectively) indicate the maximum flow rates of CO_2 through each system, relative to the flow rate of CO_2 in the flue gas of the CPP. The physical components of the capture system (number of absorption trays, solvent flow rate, etc.) are not determined by the model directly. Instead, the CO_2 flow rates are used to match the system to an interpolation of the IECM 8.0.2 model output, which is in turn used to estimate the capital cost of the system. The decision variable for the solvent storage system ($x_{Size,Stor}$) is the maximum CO_2 storage capacity of the tank[3] in kg.

The operations are dependent on a nonlinear combination of all other design and operation variables. With one additional operational decision variable set that indicates the amount of CO_2-rich amine to put into storage in a given time step ($\mathbf{u}_{Cap-Stor}$), the complete capture system operations can be calculated. The model for the capture system is similar to that described in Kang et al. [12], though there are some differences. Specifically, in Kang et al. the regeneration unit is sized relative to the auxiliary natural gas system. Here, by contrast, the sizes of the absorption, regeneration, and storage systems are all decision variables. Consequently, in this work the steam utilization in the capture system is also impacted by the sizes of the absorption and regeneration systems, and this requires us to introduce some modifications into the capture model.

As noted above, capital costs for the absorption and regeneration systems are based on IECM 8.0.2. Reference PECs, sizes, and scaling factors are determined by running IECM 8.0.2 for a variety of different flue gas flow rates, and then extracting the reported capital cost information for each system. The costs for the regeneration and compression systems are coupled, as the units scale together. Storage tank costs are based on data provided by Ulrich and Vasudevan [19]. A solvent cost of 1.98 USD/kg MEA is also incorporated. PECs are reported in Table 6. While the value for α for solvent storage tanks is below 1, this factor applies to individual tanks. When the necessary tank capacity, often in the tens of thousands of cubic meters, exceeds the maximum size (7000 m^3), multiple tanks are used and the scaling becomes essentially linear.

[3] This capacity is of a single tank, though in reality, there are two tanks: one for lean solvent and one for rich solvent. The capital costs include both tanks.

3. Optimization methodology

Computational optimization is applied to maximize the NPV of the facility over its operating life. NPV is a function of the design ($\mathbf{x}$) and operational decision variables ($\mathbf{u}$) as follows:

$$\mathrm{NPV} = -C(\mathbf{x}) + \sum_{\tau=1}^{N_{years}} \frac{P(\mathbf{x},\mathbf{u})}{(1-r)^{\tau}} \tag{3}$$

where C is the capital cost of the design and P is the profit in year τ. The real discount rate (r) accounts for the time value of money over the lifetime (N_{years}) of the system, here taken to be 30 years. The complete optimization problem is given by:

$$\max_{\mathbf{x}\in X,\mathbf{u}\in U} \mathrm{NPV}(\mathbf{x},\mathbf{u}) \tag{4}$$

subject to:

$$\mathbf{h}_{des}(\mathbf{x}) \le \mathbf{0},\ \mathbf{h}_{op}(\mathbf{x},\mathbf{u}) \le \mathbf{0} \tag{5}$$

where $\mathbf{h}_{des}$ and $\mathbf{h}_{op}$ are the nonlinear constraint violations of the design and operations optimization respectively, and X and U define the allowable values for $\mathbf{x}$ and $\mathbf{u}$ respectively.

Equation (4) subject to Equation (5) is solved using a two-level approach, outlined in Fig. 3, similar to the method presented by Bellout et al. [29]. This corresponds to the solution of the following optimization problem:

Table 5
Capture system duty requirements.

Duty type	Duty	Units
Regenerator heat	3680	kJ_{th}/kg CO_2
Compressor work	335	kJ_e/kg CO_2
Pump work	40	kJ_e/kg CO_2

Table 6
Capture system PEC data.

System	S_{ref}	PEC_{ref}	α
Absorption	150 kg/s	145×10^6 USD	0.88
Regen. & Comp.	150 kg/s	175×10^6 USD	0.85
Amine storage	7000 m^3	1.3×10^6 USD	0.88

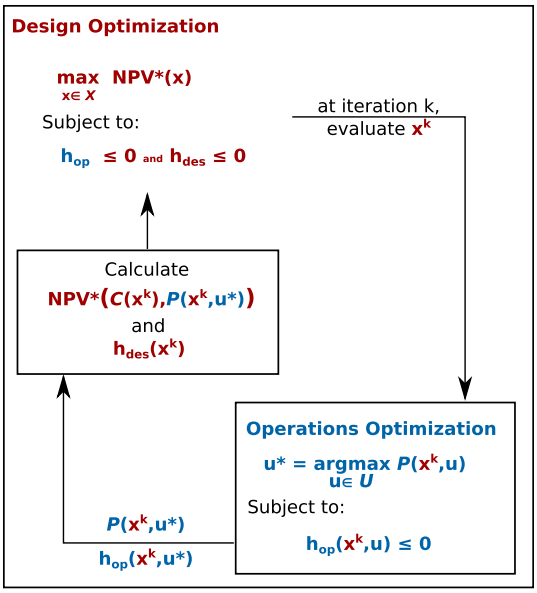

Fig. 3. Optimization methodology, with the goal of maximizing NPV as a function of capital cost (C) and annual profit (P), subject to the constraint violations ($\mathbf{h}_{des}$ and $\mathbf{h}_{op}$).

$$\max_{\mathbf{x}\in X} \max_{\mathbf{u}\in U} \text{NPV}(\mathbf{x},\mathbf{u}) \tag{6}$$

In the outer level, the design variables $\mathbf{x}$ are assigned. The current design[4] $\mathbf{x}^k$ is then used in the inner-level optimization, where the operation variables $\mathbf{u}$ are computed to maximize the profit for $\mathbf{x}^k$ over the course of a year. The yearly profit, along with the capital investment associated with design $\mathbf{x}^k$, is then used at the outer level to compute the maximum NPV for design $\mathbf{x}^k$, which we designate NPV*. Through successive iterations between levels, the optimal NPV and the associated $\mathbf{x}$ and $\mathbf{u}$ are obtained. We now describe the outer and inner optimization levels, which we refer to as the design and operations optimization, in more detail.

3.1. Design optimization

The eight design decision variables contained in $\mathbf{x}$ are summarized in Table 7. The design problem includes integer and continuous variables that combine in a nonlinear manner, making this a MINLP (mixed integer nonlinear programming) problem. The design optimization maximizes NPV*; i.e.,

$$\max_{\mathbf{x}\in X} \text{NPV}^*(\mathbf{x}) \tag{7}$$

subject to the design constraint in Equation (5). Note that NPV* for a given $\mathbf{x}$ is determined in the operations optimization.

A hybrid algorithm that includes PSO (Particle Swarm Optimization) and MADS (Mesh Adaptive Direct Search) is utilized to solve this problem [30,31]. The hybrid PSO-MADS algorithm combines the positive features of both optimization methods, specifically the global search character of PSO and the local convergence properties of MADS. The procedure handles nonlinear constraints using a filter-based treatment. The overall method has been shown to perform effectively for a variety of problems [13,30,31].

[4] In the optimization algorithm used in this work, many potential designs are considered simultaneously at iteration k, and each has an associated $\mathbf{u}$. For convenience, a single design $\mathbf{x}^k$ per iteration is discussed here.

Table 7
Design decision variables.

Decision variable	Description	Bounds
$x_{\text{Num,GT}}$	Number of gas turbines	0 – 3
$x_{\text{Size,GT}}$	Gas turbine capacity	1 – 300 MW
$x_{\text{Size,HRSG}}$	HRSG size[a]	64.4 – 1930 m^2/MW_e
$x_{\text{Size,Abs}}$	Absorption system size[b]	0 – 0.9
$x_{\text{Size,Reg}}$	Regeneration & compression system size[b]	0 – 2
$x_{\text{Size,Stor}}$	Amine storage system size	2 – 10,000 tCO_2
$x_{\text{Size,Sol}}$	Size of solar thermal parabolic troughs	0 – 8,000,000 m^2
$x_{\text{Size,Sol-ST}}$	Size of solar thermal steam turbine	0 – 1000 MW

[a] Relative to the size of the gas turbine, bounds are specific to the HRSG configuration used for an 8% discount rate (see Supplementary Information).
[b] CO_2 flow rate capacity relative to the CO_2 flow rate of the CPP.

3.2. Operations optimization

Four sets of operational decision variables $\mathbf{u}$ are determined in the operations optimization. These variables are summarized in Table 8. The optimal set of operational decision variables $\mathbf{u}^*$ for a given design $\mathbf{x}^k$ provides NPV*; i.e., $\text{NPV}^*(\mathbf{x}^k) = \text{NPV}(\mathbf{x}^k,\mathbf{u}^*)$. This value is used in the design optimization problem described above.

These optimal operation variables are determined by maximizing the annual profit of the facility as follows:

$$\max_{\mathbf{u}\in U} P(\mathbf{x},\mathbf{u}) = \sum_{t=1}^{N_t} (R_t(\mathbf{x},\mathbf{u}_t) - E_t(\mathbf{x},\mathbf{u}_t)) \tag{8}$$

where R is the revenue and E is the operating expense in any time step t. Equation (8) is solved subject to the nonlinear operational constraints in Equation (5). Constraints related to CO_2 intensity, total electricity export, and mass balances are included. Specifically, CO_2 intensities for each subsystem and for the facility as a whole are considered. As noted earlier, the system as a whole is constrained to produce less than twice the electricity provided by the CPP. Mass balance constraints ensure that the problem is physically feasible. The mass balance constraint on the storage system, which ensures that the amount of CO_2-rich amine in the storage tank is the same at the beginning and end of each day, is dependent on all four sets of operational decision variables.

The operations optimization problem is solved using the nonlinear solver SNOPT [32]. SNOPT is a local optimizer that uses a sequential quadratic programming algorithm to generate a solution based on successive quadratic estimates of the Lagrangian function under linear constraints [33]. We use numerical finite differences to construct the gradient. The Hessian is approximated using a quasi-Newton method [32].

This optimization problem is nonconvex, and multiple local optima exist. Therefore, in order to avoid poor local optima, we use multiple starting points for this optimization. The solution that provides the best NPV*, while satisfying the constraints, is chosen. Kang et al. [12] used a similar technique and achieved satisfactory results using five different starting points and ten restarts, which entailed randomly perturbing converged solutions. They optimized

Table 8
Operational decision variable sets.

Decision variable	Description	Bounds[a]
$\mathbf{u}_{\text{GT}}$	Gas turbine partial load	0–1
$\mathbf{u}_{\text{Sol}}$	Solar thermal steam production fraction	0–1
$\mathbf{u}_{\text{Sol-ST}}$	Solar thermal steam turbine utilization fraction	0–1
$\mathbf{u}_{\text{Cap-Stor}}$	Capture system storage fraction	0–1

[a] Bounds are a fraction of the maximum capacity of the subsystem, determined by the corresponding design decision variable(s).

over only a single day, however, in contrast to the multi-day optimizations used here. Consequently, in this work we use 100 random starting points for our determination of $\mathbf{u}^*$ (and NPV*).

Ideally, facility operations would be optimized on an hourly basis over the lifetime of the system. Due to the computational enormity of such a problem, a series of simplifications are introduced to reduce the problem to a reasonable size. The first simplification is to perform the optimization over only a single year. The single-year results are then applied, with appropriate discounting, over the 30-year time period in Equation (3). The second simplification is to perform the optimization on two-hour time steps, which reduces by a factor of two the number of hourly decision variables. The final simplification is to generate a subset of days, which are representative of the entire year, and to optimize over only these days. The methodology for choosing this subset of days is described in the next section.

4. Generation of statistically representative days

Optimizing the operations for a single day requires solving a set of four operational decision variables for each model time step. Each day is discretized into 12 two-hour time steps. Of the 48 resulting operational variables for each day, approximately eight (depending on the day) are known *a priori* as they correspond to time periods without solar irradiation, reducing the problem to 40 variables. There are 15 nonlinear constraints required to enforce mass and energy balances of the system. The constraints for CO_2 emissions and maximum electricity production couple the days together, meaning that the difficulty of the optimization grows with the number of days considered. Our optimization algorithm was found to be capable of consistently solving this problem with up to 8 days, or 320 variables and 108 nonlinear constraints. Consequently, in order to evaluate the optimal profit from the facility for an entire year, the problem must be reduced in scale substantially.

The two time-dependent data sets used in this problem are wholesale electricity clearing price (USD/MWh) and global minus diffuse irradiation (Wh/m^2, referred to simply as irradiation hereafter). Electricity prices from the California Independent System Operator OASIS database [34], and irradiation data from near Farmington, New Mexico, are used. Irradiation data are obtained from the NSRDB [35] (National Solar Radiation Data Base) maintained by the National Renewable Energy Laboratory. Both electricity and solar data are from 2010, as this is the most recent year available from the NSRDB. Daily data averaged over two-hour periods are shown in Fig. 4(a).

It is necessary to consider both data sets together in order to preserve any existing correlations. We represent each day in 2010 as a 24-element vector, with the first 12 elements corresponding to electricity price and the last 12 to irradiation. K-means clustering is used to group the days, by minimizing the SSE (sum of squared error) between the representative days (cluster centroids) and the yearly data. In the SSE calculation, equal weight is given to both the irradiation and electricity portion of each vector. This is accomplished by scaling the irradiation components such that the year-average positive irradiation is equal to the year-average electricity price. The K-means clustering algorithm groups the data vectors around the cluster centroid values, and consequently preserves the mean of each element of the vector [36]. K-means clustering is sensitive to the initial guess. We thus apply clustering 10,000 times using random starting points, and select the result with the lowest SSE, as suggested by Su and Dy [37].

The required number of representative days is determined by condensing the data into successively increasing numbers of days and comparing the results. The normalized SSE between the clustered and actual days is shown in Fig. 5(a). In order to determine if the features of the data that most strongly impact the optimization are captured, we performed optimizations using different numbers of representative days. Fig. 5(b) shows the results of the optimization for both a gas-only and a solar-only design. In each case, the gas price was fixed at 6.5 USD/GJ, and the electricity price was 1.5 times the 2010 electricity price.

The results show opposite trends for gas and solar thermal designs. The increase in NPV with the number of representative days in the gas designs results because the gas system is able to take advantage of the increased variability in electricity prices. The gas turbine capacity selected by the optimization algorithm is sufficiently large that it can reduce the partial load during hours in which the electricity price is so low that the system does not profit from electricity sales, while still providing enough steam for the capture system to satisfy the CO_2 emissions constraint. The decrease in NPV in the solar designs with increasing numbers of representative days is due to the increased variability in irradiation. The optimal solar design with each number of representative days involves the utilization of the amine storage system. As variability increases, either the relative utilization of the storage system must decrease, or the relative oversizing of the solar thermal field must increase. In either case, the utilization of capital decreases, and consequently so does the NPV.

Fig. 5(a) shows that the use of 6 representative days reduces the normalized SSE to acceptable levels. Fig. 5(b) indicates that at least 6 representative days are required in order for the NPV of both solar and natural-gas-based designs to stabilize. Therefore, in all subsequent optimizations, we use 6 representative days, with appropriate weightings, to represent the days of the year. Fig. 4(b) shows these 6 days (which correspond to the centroids of the 6 clusters), along with the fraction of the year that each day represents. The dates listed in Fig. 4(b) indicate the day of the year that is closest to each cluster centroid.

5. Optimization results

Two parameters that strongly impact NPV are the electricity and natural gas prices. Both of these prices are uncertain, particularly when considering the lifetime of the power plant. Rather than attempt to predict future energy markets, we explore a large domain of reasonable scenarios and identify trends in the optimization results. Natural gas prices between 3 and 10 USD/GJ, and electricity prices ranging from the 2010 electricity price to double that price (mean price from approximately 36 to 73 USD/MWh), are considered.

Other quantities that strongly influence NPV are economic incentives for solar power. A variety of such incentives exist, but here we consider only ITCs (investment tax credits) and PPAs (power purchase agreements). A 30% ITC is presently in the US tax code, and this is the ITC value used in this work (when an ITC is included). A PPA guarantees a fixed price for the electricity generated over the contract period. While PPA contracts vary widely, fixed rates of 100 and 150 USD/MWh are used in this work for simplicity.[5] Finally, the discount rate used is both influential on the system NPV, and dependent upon the financing available at a particular site. Real discount rates of 6, 8, and 10% are considered in this analysis.

Optimal facility design and operations are determined for various combinations of the economic parameters. The results can conceptually be divided into three categories: natural-gas-based systems, solar-thermal-based systems, and hybrid systems that utilize both solar and natural gas. In the results below, we first

[5] PPAs apply only to electricity produced from the solar thermal system.

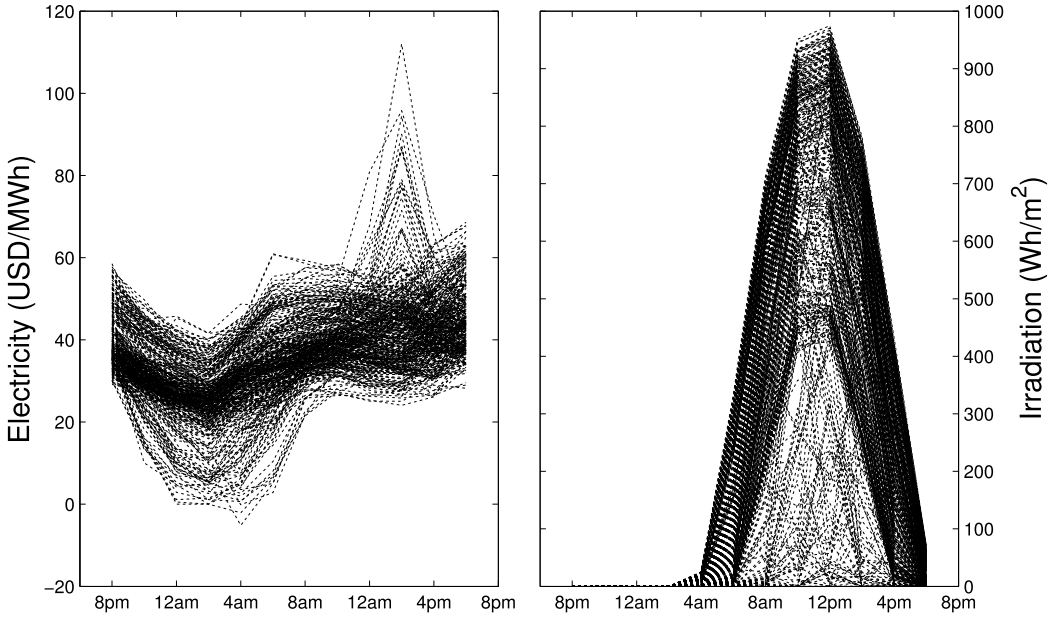

(a) Daily electricity and irradiation data, averaged over two-hour periods.

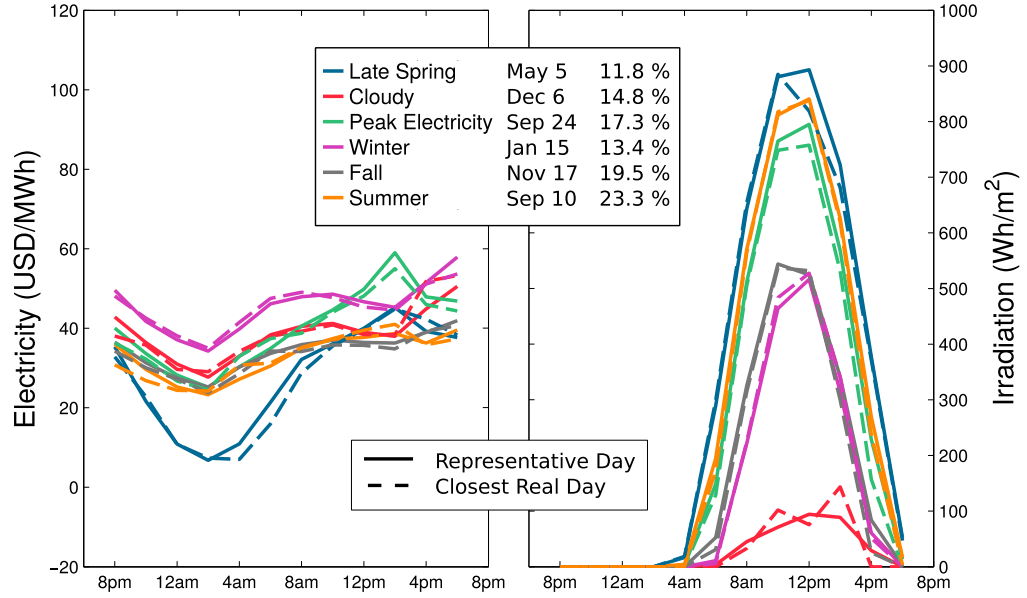

(b) Clustered electricity and irradiation data with solid lines indicating representative days and dashed lines indicating the closest real day to each cluster. The legend identifies the real day and shows the fraction of the year each cluster represents.

Fig. 4. Daily (a) and clustered (b) electricity and irradiation data.

examine a base case, then explore the effects of several different parameters, and then vary several of the key parameters simultaneously.

5.1. Base case

For the base case, we specify a natural gas price of 6.5 USD/GJ, an average wholesale electricity price of 54.5 USD/MWh (determined by multiplying the 2010 representative-day electricity prices by 1.5), a 30% solar ITC, no PPA, and an 8% real discount rate. Table 9 shows the design parameters found for both the optimal solar thermal and natural gas systems. The solar thermal configuration relies heavily upon the utilization of the amine storage system under these conditions (in fact, amine storage of various capacities appears in solar thermal designs for all economic parameters explored).

For this case, the optimal natural gas system results in an NPV of 368 million USD, while the best solar thermal system corresponds to an NPV of 82.7 million USD. Thus, although the natural gas system is optimal for the base case, the solar thermal system is still profitable (meaning it provides a positive overall NPV). Both systems suffer a loss relative to the existing CPP without retrofit, which has an NPV of 714 million USD, but of course the standalone CPP does not satisfy the CO_2 emissions constraint.

Extensive results for natural-gas-based auxiliary systems are presented in Kang et al. [13], so our focus here will be on the solar

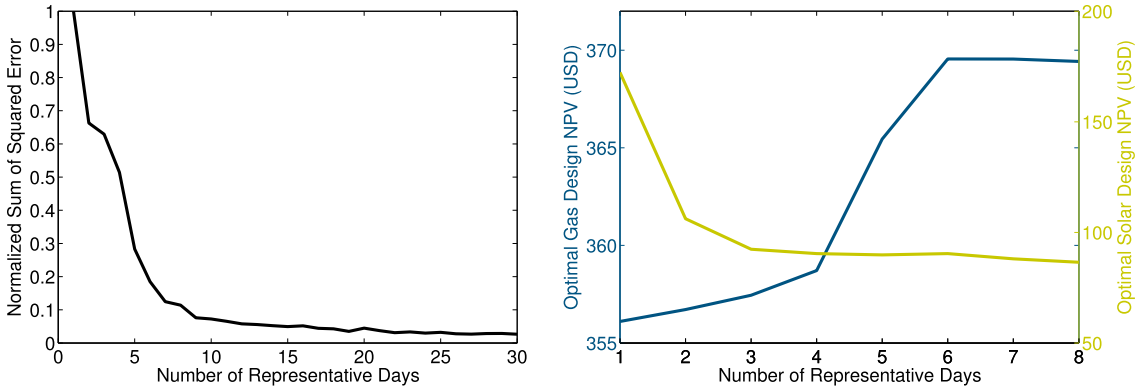

(a) SSE for different numbers of representative days.

(b) Optimal design and operations for different numbers of representative days. Gas-only optimization is in blue, and solar-thermal-only optimization is in yellow.

Fig. 5. Effects of using different numbers of representative days.

thermal system (even though, as indicated above, the natural gas system is preferred in the base case). Fig. 6(a) and (b) present the optimal operations of the CO_2 capture subsystem during the late spring and winter representative days. The green line (in web version) indicates the amount of CO_2 in storage at the end of any time step. The net CO_2 entering the storage system is the difference between the hourly absorption (in blue) and regeneration (in red). The amount of stored CO_2 is zero at the start and end of each day (8 pm), as indicated by both figures, where the amount of CO_2 in storage at the end of the first time step is equal to the amount absorbed during that time step.

Approximately four hours of storage are utilized in the optimal solar thermal design. This enables the system to absorb CO_2 at night, store the rich solvent, and then regenerate rich solvent during hours of peak irradiation. Solvent storage thus acts to time-shift the regeneration energy demand, and in this sense is analogous to energy storage. Although the amine storage system does require significant capital costs (approximately 54 million USD in this case), it actually reduces the total capital investment by enabling the use of a smaller solar field, as well as smaller regeneration, compression, and absorption systems.

The rates of absorption and regeneration in the capture system are dependent on the steam supplied by the auxiliary heat source, and for the solar design case, this depends on the amount of irradiation. Fig. 6(c) and (d) show the utilization of energy in the solar thermal system for the late spring and winter representative days. The total incident irradiation in the winter representative day is significantly less than in the late spring day, and consequently less CO_2 is captured and the CO_2 intensity from the facility is much higher. Over the course of the entire year the CO_2 intensity constraint is satisfied, even if it is not met in a particular day.

Table 9
Optimal design variables in the base case.

Decision variable	Natural gas design	Solar thermal design
$x_{Num,GT}$	1	0
$x_{Size,GT}$	300 MW	0
$x_{Size,HRSG} \times x_{Size,GT}$	217,000 m^2	0
$x_{Size,Abs} \times$ FG	52.1 kg CO_2/s	99.5 kg CO_2/s
$x_{Size,Reg} \times$ FG	52.4 kg CO_2/s	152 kg CO_2/s
$x_{Size,Stor}$	0	1510 tCO_2
$x_{Size,Sol}$	0	3.13×10^6 m^2
$x_{Size,Sol-ST}$	0	203 MW

FG designates the flow rate of CO_2 in the flue gas stream.

On days with peak irradiation, such as during the late spring day shown in Fig. 6(c), the solar thermal system produces more steam than is used by the capture system (shown in gray). This over-sizing increases the number of hours over the course of the year that steam is available, during both off-peak hours of high-irradiation days (as in Fig. 6(c)), as well as in all hours of low-irradiation days (as in Fig. 6(d)). However, the over-sizing also results in incomplete steam utilization, which accounts for approximately 19% of the total available energy from steam in the base case. We note that (essentially) all steam is passed through the turbine for electricity generation, even if it is not subsequently used for CO_2 regeneration (in which case the steam is simply condensed and the water is reused).

While the base case design and operations are a robust solution obtained from numerous optimization runs involving many thousands of candidate designs, interpretations of these results are inherently complex. However, the results indicate that in order to satisfy the CO_2 constraint with solar thermal energy that is variable on both daily and seasonal time-scales, some component over-sizing is necessary. Of the many possible combinations of component sizes, it is evident that an over-sized solar thermal array has the highest NPV (in the base case), most likely because it not only satisfies the emissions constraint, but also increases the system electricity production.

5.2. Parametric study

The base case results for both the natural gas and solar thermal systems are highly dependent on the economic parameters. Fig. 7 shows the influence of each of the parameters individually on the optimal NPVs. To obtain the NPV range for a given parameter, the parameter is varied while all of the others are held constant, and the full optimization is performed for each case. The range over which each parameter is varied is indicated in Fig. 7. The NPV ranges for some of the parameters are very wide, and they differ substantially between the natural-gas and solar-thermal-based systems. Within the ranges explored, the most influential parameters are mean electricity clearing price and natural gas price.

We demonstrate the effect of varying these two parameters together by presenting optimization results on a two-dimensional price plane. Fig. 8 shows two such planes around the base case – one corresponds to a 30% ITC (the base case), and one does not include any ITC. The color (in web version) in a given area of Fig. 8 indicates which design has a higher NPV (this is the preferred

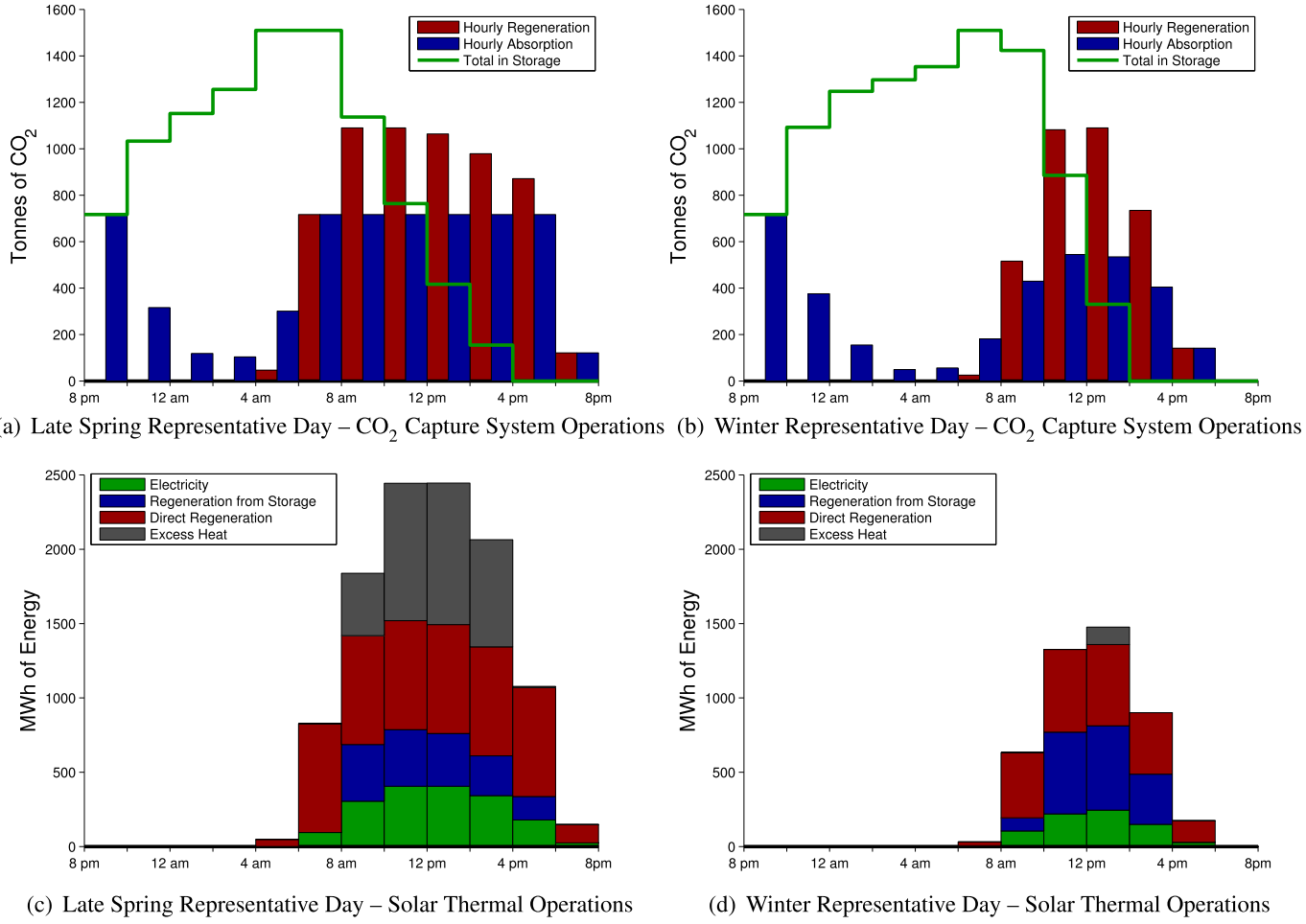

Fig. 6. Operations of the solar thermal and CO_2 capture system in the optimal solar design for the base case.

design), with yellow, blue, and green indicating solar thermal, natural gas, and hybrid designs respectively. The cross-hatched area shows the region where neither system has a positive NPV under the CO_2 constraint, indicating that shutting down the facility would be the economically optimal choice. It is important to emphasize that

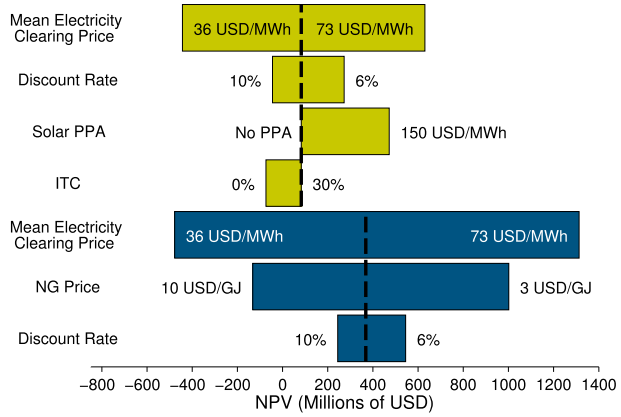

Fig. 7. Influence of different economic parameters on NPV. Blue and yellow bars indicate systems utilizing natural gas and solar thermal auxiliary systems, respectively. The black dashed lines show the optimal NPV for the base case for both systems. (For interpretation of the references to color in this figure legend, the reader is referred to the web version of this article.)

each of the colored blocks in Fig. 8 (and in subsequent figures of this type) is derived from a full optimization run, and each corresponds to a particular design and set of operating variables.

We see from the left-hand side of Fig. 8 that without any solar incentives, natural-gas-based designs are always preferred when the system is profitable. A 30% solar ITC, shown in the right-hand side of Fig. 8, introduces a preference in some regions towards designs with solar-thermal components, some of which are hybrid designs. Specifically, in the case of a 30% ITC, medium to high electricity prices, and natural gas prices exceeding 8.5 USD/GJ, solar-thermal-only auxiliary systems are preferred.

Fig. 8 and subsequent figures indicate the preferred system, and whether or not it is profitable, but they do not provide quantitative information on NPV, capital cost, and the relative advantage of the optimal system over alternate systems. This information is provided in Table 10, where we give more detailed results for specific points indicated in the figures. For the selected points, the table provides data for the optimal system, as well as for alternate (nonoptimal) designs. Note that, for any case, we can "force" the optimizer to generate the best nonoptimal gas-only or solar-only system, but not the best nonoptimal hybrid system (since in this case the optimizer would simply converge to either a gas-only or solar-only system). Therefore, hybrid systems only appear in Table 10 when they are the optimal result.

For point b in Fig. 8, Table 10 shows an NPV of 1.1 million USD for a natural-gas-based system, and an NPV of 82.7 million USD for a solar-thermal-based system, meaning solar thermal is strongly

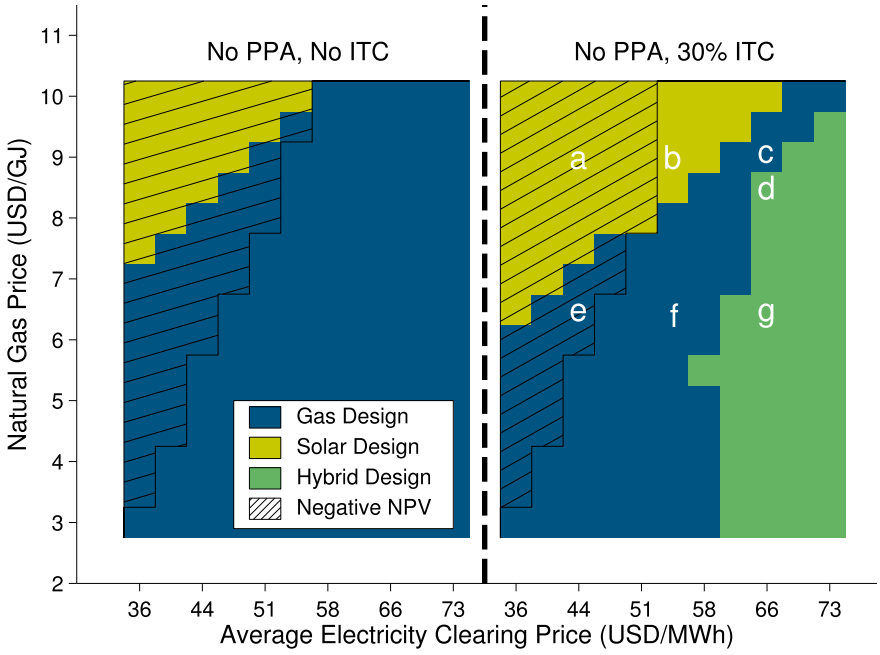

Fig. 8. Design preference under an 8% real discount rate with and without a solar ITC. Letters refer to scenarios quantified in Table 10.

preferred. This wide of a margin in NPV does not occur in all cases, however. For example, comparing the hybrid and gas-only systems at point g in Fig. 8, we see an NPV difference of only 8 million USD, despite very different designs (evidenced by the 94 million USD difference in capital costs). For point d, the advantage of the hybrid system over the gas-only system is even less – only 1 million USD. In this case it is unlikely that the hybrid system would be built, since there are presumably additional costs associated with the added complexity of operating a hybrid system that are not incorporated into our analysis.

While the NPV of the retrofit (i.e., the facility excluding coal plant power sales and costs) is negative in all cases in Fig. 8, there are some regions where an incremental increase in electricity production increases the NPV of the facility. The hybrid designs shown in the high electricity price regime under the 30% ITC result from this effect. In these hybrid designs, solar thermal steam production partially replaces the CCS heat demand from the gas-fired subsystem, enabling increased electricity production from the gas-fired subsystem. Points c and d in Table 10 highlight the benefit of a hybrid system over a gas-only system.

Table 10
Results of selected economic points.

Point (Figure)	Electricity price (USD/MWh)	Gas price (USD/GJ)	PPA (USD/MWh)	Design type	NPV (10^6 USD)	Capital cost (10^6 USD)	Operating profit (10^6 USD/year)	Gas use (10^6 GJ/year)
a (8)	44	9	None	Gas	−497	408	−22.4	637
e (8)	44	6.5	None	Gas	−139	408	27.1	638
a/e (8)	44	Any	None	Solar	−235	924	58.4	0
b* (8)	54.5	9	None	Gas	1.1	413	60.8	638
f† (8)	54.5	6.5	None	Gas	368	453	115	776
b/f (8)	54.5	Any	None	Solar	82.7	953	105	0
c (8)	66	9	None	Gas	519	410	131	637
d (8)	66	8.5	None	Gas	591	412	129	638
d (8)	66	8.5	None	Hybrid	592	501	136	631
g (8)	66	6.5	None	Gas	933	462	195	788
g (8)	66	6.5	None	Hybrid	941	556	204	788
c/d/g (8)	66	Any	None	Solar	411	992	168	0
h* (9)	54.5	9	–	Gas	1.1	413	60.8	638
h (9)	54.5	9	100	Hybrid	146	984	115	215
i† (9)	54.5	6.5	–	Gas	368	453	115	776
i (9)	54.5	6.5	100	Hybrid	385	690	124	729
h/i (9)	54.5	Any	100	Solar	183	1220	140	0
j* (9)	54.5	9	–	Gas	1.1	413	60.8	638
j (9)	54.5	9	150	Hybrid	463	1640	212	179
k† (9)	54.5	6.5	–	Gas	368	453	115	776
k (9)	54.5	6.5	150	Hybrid	558	1280	198	748
j/k (9)	54.5	Any	150	Solar	473	1760	225	0

*/† – Since gas-only-designs are independent of any PPA, the gas-only-designs at points b, h, and j (designated by *) are the same, and gas-only designs at points f, i, and k (designated by †) are the same.
All values shown reflect an ITC value of 30% and a real discount rate of 8%.

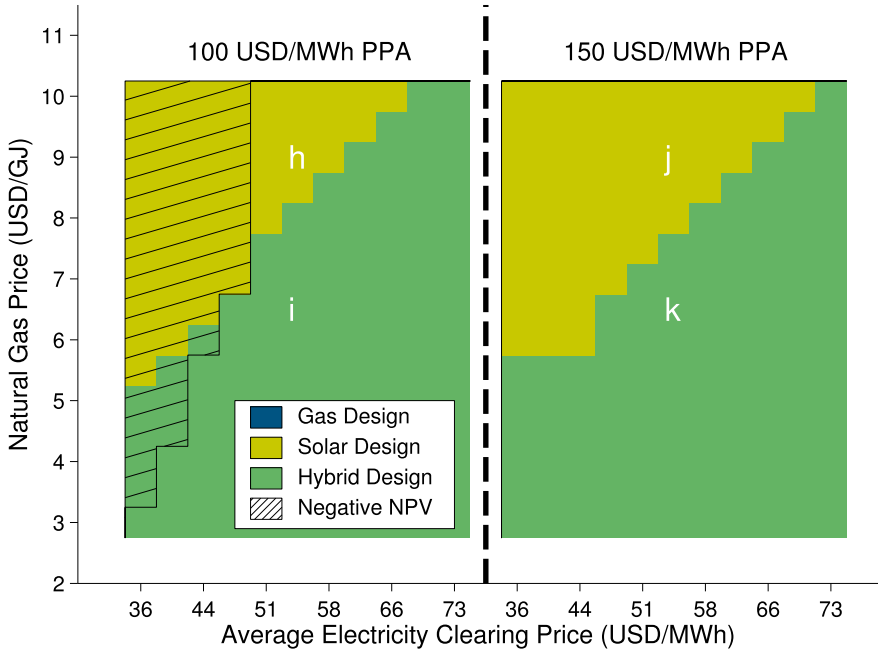

Fig. 9. Design preference under an 8% real discount rate with two different solar PPAs (and a 30% ITC). Letters refer to scenarios quantified in Table 10.

Solar thermal designs can be further incentivized with PPAs. Fig. 9 presents optimized outcomes under two different PPAs (100 and 150 USD/MWh). Comparing the different plots makes it apparent that the choice of system design is highly sensitive to a PPA, and high enough rates can make designs incorporating solar thermal preferable at all conditions explored, even at low gas prices. Table 10 demonstrates that very high PPAs lead to a drastic increase in both the NPV and capital cost of the optimal system. Points i and k, for example, quantify the increase in NPV and capital cost as we proceed from a PPA of 100 to 150 USD/MWh. Note, however, that the emphasis of the design at these high PPAs is not on producing steam for carbon capture, but instead on directly producing electricity.

Finally, a small change in discount rate can have a substantial effect on NPV, an effect which is not equal for the two types of designs. Fig. 10 shows results for real discount rates of 6, 8, and 10%,

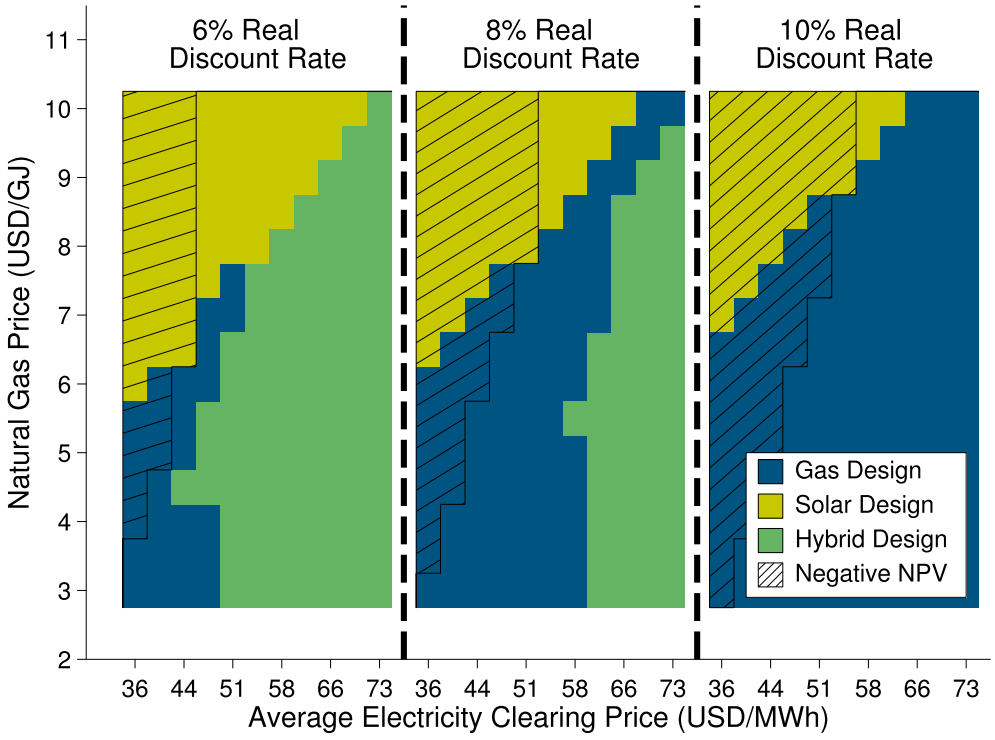

Fig. 10. Design preference under various discount rates, electricity prices and gas prices, with a fixed solar ITC of 30% and no PPA.

coupled with the variation in natural gas and electricity prices. High discount rates favor systems with low capital costs, while low discount rates favor systems with lower operating costs. As the discount rate decreases, more of the economic plane becomes profitable, and designs with a solar thermal component (which require high capital investment but have low operating costs relative to gas) become more favorable.

6. Concluding remarks

In this work, we developed an optimization procedure to determine the optimal design and operations of carbon capture retrofits to coal-fired power plants. An amine-based temperature-swing absorption system was considered for CO_2 capture. The goal of the optimizations was to maximize the NPV while satisfying an annual average emissions constraint. We analyzed two methods for providing auxiliary heat for the capture system, one using a natural-gas-based system, and the other using a solar-thermal-based system. A two-level optimization procedure was used to evaluate both the design and the time-dependent operations of the facility. The approach uses both gradient and stochastic optimization techniques. A variety of economic scenarios were assessed to determine which conditions favored natural gas and which favored solar-thermal-based designs.

This analysis demonstrates the wide domain of parameters that influence both the NPV and the design choices for a carbon capture retrofit that utilizes auxiliary heat. Our results show that, without any solar incentives, natural-gas-based systems are always preferred for systems with a positive NPV. With a 30% ITC, 7.5 USD/GJ or higher natural gas prices, mean electricity clearing prices above 47 USD/MWh, and real discount rates at or below 8%, solar-thermal-only designs are commonly preferred. With high electricity prices and real discount rates at or below 8%, hybrid designs become preferable even when the natural-gas price is low, because the solar-thermal steam allows for an increase in electricity production from the gas-fired subsystem. Finally, with the introduction of a solar PPA at or above 100 USD/MWh, designs with some solar thermal component (either hybrid or solar-only) are always preferred. It is also important to note that solar thermal designs are profitable in many scenarios even though natural gas is preferable (optimal). In regions of the world where natural gas is not available, solar thermal can represent a profitable design (depending on the discount rate, and assuming an increase in electricity prices from 2010 levels of 40–60%).

This work can be extended in a number of useful directions. Current work includes enhancing the modeling capabilities of the capture subsystem to include decision variables for specific physical components. Many other scenarios could be readily explored with the existing implementation. These could include, for example, consideration of other sites for power generation and solar-thermal-based carbon capture, other electricity markets, and different policy frameworks (such as a carbon tax). Although the solar thermal system considered here is commercially available, it was not specifically designed for use in CO_2 capture (its original application area is enhanced oil recovery). Thus, it would be of interest to consider solar thermal designs that provide steam at the conditions required for amine-based capture, or to incorporate the detailed solar thermal design into the overall optimization. This might render solar thermal systems preferable over a larger range of economic conditions. Other processes for CO_2 capture could additionally be considered. Finally, because the optimizations are quite demanding computationally, it may also be of use to explore alternative (local and global) optimization strategies.

Acknowledgments

We thank John O'Donnell (GlassPoint) for providing us with information and specifications on the solar thermal system, and Obiajulu Isebor (now at BP) for his assistance with the optimization algorithms. The Stanford Center for Computational Earth and Environmental Science provided the computational resources used in this work. The first author thanks the William Bourne Fellowship, and the second author thanks the Illich-Sadowsky Stanford Interdisciplinary Graduate Fellowship, for financial support.

Nomenclature

ABTSA	amine-based temperature-swing absorption
CCS	carbon capture and storage
CPP	coal-fired power plant
HHV	higher heating value
HRSG	heat recovery steam generator
ITC	investment tax credit
NPV	net present value
NPV^*	maximum NPV for a given design
PEC	purchased equipment cost
PPA	power purchase agreement
SSE	sum of squared error
C	capital cost
$\dot{E}$	gas turbine output work
E	operating expense
L	gas turbine partial load
N_{years}	system lifetime for NPV calculation
P	profit
PEC_{ref}	reference component PEC
R	revenue
S	component size
S_{ref}	reference component size
$\mathbf{h}_{\text{des}}$	constraint violations of the design optimization
$\mathbf{h}_{\text{op}}$	constraint violations of the operations optimization
$\dot{m}_g$	gas turbine flue gas flow rate
r	real discount rate
$\mathbf{u}$	operational decision variables
$\mathbf{u}_{\text{Cap}-\text{Stor}}$	fraction of CO_2-rich amine to put into storage in a given time step
$\mathbf{u}_{\text{GT}}$	gas turbine partial load
$\mathbf{u}_{\text{Sol}-\text{ST}}$	solar thermal steam turbine utilization fraction
$\mathbf{u}_{\text{Sol}}$	solar thermal steam production fraction
$\mathbf{x}$	design decision variables
$x_{\text{Size,Abs}}$	maximum CO_2 flow rate in the absorption system, relative to the CO_2 flow rate in the CPP flue gas
$x_{\text{Size,GT}}$	gas turbine capacity
$x_{\text{Size,HRSG}}$	HRSG size relative to gas turbine capacity
$x_{\text{Size,Reg}}$	maximum CO_2 flow rate in the regeneration system, relative to the CO_2 flow rate in the CPP flue gas
$x_{\text{Size,Sol}-\text{ST}}$	size of solar thermal wet steam turbine
$x_{\text{Size,Sol}}$	size of solar thermal parabolic troughs
$x_{\text{Size,Stor}}$	amine system storage size in terms of CO_2
α	PEC component scaling factor
Δh_g	natural gas HHV
η_{rel}	gas turbine partial load efficiency
η_{th}	gas turbine design thermal efficiency
τ	year in NPV calculation

Appendix A. Supplementary information

Supplementary data related to this article can be found at http://dx.doi.org/10.1016/j.energy.2014.11.003.

References

[1] International Energy Agency. Technology roadmap: carbon capture and storage. 2013. Tech. Rep.

[2] Boot-Handford ME, Abanades JC, Anthony EJ, Blunt MJ, Brandani S, Mac Dowell N, et al. Carbon capture and storage update. Energy Environ Sci 2014;7(1):130. http://dx.doi.org/10.1039/c3ee42350f.

[3] Herzog H, Meldon J, Hatton A. Advanced post-combustion CO_2 capture, prepared for the clean air task force. 2009. Tech. Rep.

[4] DOE and NETL. Cost and performance baseline for fossil energy plants, vol. 1; 2013. Bituminous coal and natural gas to electricity final report DOE/NETL–2010/1397, Tech. Rep.

[5] Metz B, editor. Carbon dioxide capture and storage: special report of the Intergovernmental Panel on Climate Change, Cambridge University Press; 2005.

[6] Stone EJ, Lowe JA, Shine KP. The impact of carbon capture and storage on climate. Energy Environ Sci 2009;2(1):81–91. http://dx.doi.org/10.1039/b807747a.

[7] Chalmers H, Lucquiaud M, Gibbins J, Leach M. Flexible operation of coal fired power plants with postcombustion capture of carbon dioxide. J Environ Eng 2009;135(6):449–58. http://dx.doi.org/10.1061/(ASCE)EE.1943-7870.0000007.

[8] Cohen SM, Rochelle GT, Webber ME. Optimizing post-combustion CO_2 capture in response to volatile electricity prices. Int J Greenh Gas Control 2012;8:180–95. http://dx.doi.org/10.1016/j.ijggc.2012.02.011.

[9] Mac Dowell N, Shah N. Identification of the cost-optimal degree of CO_2 capture: an optimisation study using dynamic process models. Int J Greenh Gas Control 2013;13:44–58. http://dx.doi.org/10.1016/j.ijggc.2012.11.029.

[10] Khalilpour R. Multi-level investment planning and scheduling under electricity and carbon market dynamics: retrofit of a power plant with PCC (post-combustion carbon capture) processes. Energy 2014;64:172–86. http://dx.doi.org/10.1016/j.energy.2013.10.086.

[11] Bashadi S, Herzog H. Using auxiliary gas power for CCS energy needs in retrofitted coal power plants. Energy Procedia 2011;4:1828–34. http://dx.doi.org/10.1016/j.egypro.2011.02.060.

[12] Kang CA, Brandt AR, Durlofsky LJ. Optimal operation of an integrated energy system including fossil fuel power generation, CO_2 capture and wind. Energy 2011;36(12):6806–20. http://dx.doi.org/10.1016/j.energy.2011.10.015.

[13] Kang CA, Brandt AR, Durlofsky LJ. Optimizing heat integration in a flexible coal-natural gas power station with CO_2 capture. Int J Greenh Gas Control 2014;31:138–52. http://dx.doi.org/10.1016/j.ijggc.2014.09.019.

[14] Cohen SM, Webber ME, Rochelle GT. Utilizing solar thermal energy for post-combustion CO_2 capture. J Energy Power Eng 2011;5:195–208.

[15] Li H, Yan J, Campana PE. Feasibility of integrating solar energy into a power plant with amine-based chemical absorption for CO_2 capture. Int J Greenh Gas Control 2012;9:272–80. http://dx.doi.org/10.1016/j.ijggc.2012.04.005.

[16] Mokhtar M, Ali MT, Khalilpour R, Abbas A, Shah N, Hajaj AA, Armstrong P, Chiesa M, Sgouridis S. Solar-assisted post-combustion carbon capture feasibility study. Appl Energy 2012;92:668–76. http://dx.doi.org/10.1016/j.apenergy.2011.07.032.

[17] Rubin ES, Berkenpas MB, Zaremsky CJ. User manual: integrated environmental control model. Tech. Rep. 2007., http://www.cmu.edu/epp/iecm.

[18] Berkenpas MB. IECM technical documents final report. November 2009. Tech. Rep.

[19] Ulrich G, Vasudevan P. Chemical engineering process design and economics: a practical guide. 2nd ed. Durham, New Hampshire, USA: Process Publishing; 2004.

[20] Ulrich G, Vasudevan P. Capital costs quickly calculated: estimating capital costs early can prevent unnecessary expenditures on dead-end projects. Chem Eng 2009:46–52.

[21] Couper J, Hertz D, Smith F. Process economics. In: Perry's Chem. Eng. Handb.. 8th ed.vol. 9. New York: McGraw-Hill; 2007. 9:1–9:56.

[22] Internal Revenue Service, United States Department of the Treasury. Publication 946: how to depreciate property. 2013. http://www.irs.gov/pub/irs-pdf/p946.pdf.

[23] Kim TS. Comparative analysis on the part load performance of combined cycle plants considering design performance and power control strategy. Energy 2004;29(1):71–85. http://dx.doi.org/10.1016/S0360-5442(03)00157-9.

[24] Farmer R, editor. Gas turbine world: 2010 GTW handbook, vol. 28; 2010. Southport.

[25] Casarosa C, Donatini F, Franco A. Thermoeconomic optimization of heat recovery steam generators operating parameters for combined plants. Energy 2004;29(3):389–414. http://dx.doi.org/10.1016/S0360-5442(02)00078-6.

[26] Bierman B, O'Donnell J, Burke R, McCormick M, Lindsay W. Construction of an enclosed trough EOR system in south Oman. Energy Procedia 2014;49:1756–65. http://dx.doi.org/10.1016/j.egypro.2014.03.186.

[27] Bierman B, Treynor C, O'Donnell J, Lawrence M, Chandra M, Farver A, et al. Performance of an enclosed trough EOR system in south Oman. Energy Procedia 2014;49:1269–78. http://dx.doi.org/10.1016/j.egypro.2014.03.136.

[28] Personal communications with John O'Donnell. Mar. 13 and Nov. 7 2013.

[29] Bellout MC, Echeverría Ciaurri D, Durlofsky LJ, Foss B, Kleppe J. Joint optimization of oil well placement and controls. Comput Geosci 2012;16(4):1061–79. http://dx.doi.org/10.1007/s10596-012-9303-5.

[30] Isebor OJ, Durlofsky LJ, Echeverría Ciaurri D. A derivative-free methodology with local and global search for the constrained joint optimization of well locations and controls. Comput Geosci 2014;18:463–82. http://dx.doi.org/10.1007/s10596-013-9383-x.

[31] Isebor OJ, Echeverría Ciaurri D, Durlofsky LJ. Generalized field-development optimization with derivative-free procedures. SPE J 2014;19:891–908. http://dx.doi.org/10.2118/163631-PA.

[32] Gill PE, Murray W, Saunders MA. SNOPT: an SQP algorithm for large-scale constrained optimization. SIAM Rev 2005;47(1):99–131. http://dx.doi.org/10.1137/S0036144504446096.

[33] Gill PE, Murray W, Saunders MA. User's guide for SNOPT version 7: software for large-scale nonlinear programming. Tech. Rep. 2008., http://citeseerx.ist.psu.edu/viewdoc/summary?doi=10.1.1.217.5929.

[34] California Independent System Operator. Open access same-time information system day ahead market locational market price query. 2010. http://oasis.caiso.com.

[35] Wilcox S. National solar radiation database 1991-2010 update: users manual. August 2012. Tech. Rep.

[36] Steinhaus H. Sur la division des corp materiels en parties. Bull Pol Acad Sci 1956:801–4.

[37] Su T, Dy J. A deterministic method for initializing K-means clustering. In: 16th IEEE Int. Conf. Tools with Artif. Intell. IEEE Comput. Soc; 2004. p. 784–6. http://dx.doi.org/10.1109/ICTAI.2004.7.